

# PeakNet: Bragg peak finding in X-ray crystallography experiments with U-Net

Cong Wang

Linac Coherent Light Source  
SLAC National Accelerator Laboratory  
cwang31@slac.stanford.edu

Po-Nan Li

Department of Electrical Engineering  
Stanford University  
liponan@stanford.edu

Jana Thayer

Linac Coherent Light Source  
SLAC National Accelerator Laboratory  
jana@slac.stanford.edu

Chun Hong Yoon

Linac Coherent Light Source  
SLAC National Accelerator Laboratory  
yoon82@slac.stanford.edu

**Abstract**—Serial crystallography at X-ray free electron laser (XFEL) sources has experienced tremendous progress in achieving high data rate in recent times. While this development offers potential to enable novel scientific investigations, such as imaging molecular events at logarithmic timescales, it also poses challenges in regards to real-time data analysis, which involves some degree of data reduction to only save those features or images pertaining to the science on disks. If data reduction is not effective, it could directly result in a substantial increase in facility budgetary requirements, or even hinder the utilization of ultra-high repetition imaging techniques making data analysis unwieldy. Furthermore, an additional challenge involves providing real-time feedback to users derived from real-time data analysis. In the context of serial crystallography, the initial and critical step in real-time data analysis is finding X-ray Bragg peaks from diffraction images. To tackle this challenge, we present PeakNet, a Bragg peak finder that utilizes neural networks and runs about four times faster than Psocake peak finder, while delivering significantly better indexing rates and comparable number of indexed events. We formulated the task of peak finding into a semantic segmentation problem, which is implemented as a classical U-Net architecture. A key advantage of PeakNet is its ability to scale linearly with respect to data volume, making it well-suited for real-time serial crystallography data analysis at high data rates.

## I. INTRODUCTION

Serial femtosecond crystallography (SFX) with X-ray free electron lasers (XFEL) has enabled structural determination of macromolecules by outrunning radiation damage at room temperature, an approach commonly known as *diffraction-before-destruction* [Chapman et al., 2006, 2011, Neutze et al., 2000]. Time-resolved serial femtosecond crystallography (TR-SFX) at XFEL facilities, like the Linac Coherent Light Source (LCLS), allows the investigation of biochemical reactions with picosecond time resolution which has led to many significant structural studies [Ibrahim et al., 2020, Kern et al., 2018, Kupitz et al., 2014, Nango et al., 2016, Pande et al., 2016, Suga et al., 2017, 2020, Young et al., 2016] since the first published work at LCLS [Aquila et al., 2012]. In the meantime, the data rate at XFEL facilities have also gradually increased from hundreds of Hz to the MHz range, with the European X-ray

Free Electron Laser (EuXFEL) being the first MHz facility available to users and LCLS-II set to launch in 2023.

At the MHz data rate, novel real-time data analysis approaches are needed to tackle two major challenges that arise in SFX experiments, namely data reduction and real time feedback. Firstly, data reduction aims to veto, extract and compress scientific data by identifying important events, commonly referred to as “hits”, and vetoing irrelevant ones from terabyte per second data streams. One typical approach for SFX hit finding utilizes existing Bragg peak finders, such as the Cheetah peak finder [Barty et al., 2014], the robust peak finder [Hadian-Jazi et al., 2017], DIALS peak finder [Winter et al., 2018] or the Psocake peak finder [Shin et al., 2018]. Additionally, a neural network-based SFX hit finder was reported to achieved a processing rate of 1.3 kHz on a single GPU [Ke et al., 2018]. ORB feature extractor combined with a multilayer perceptron (MLP) hit classifier showed promising results for SFX data [Rahmani et al., 2023]. Secondly, real-time feedback in SFX experiments provides users with information on the experimental conditions and allows them to make real-time decisions that can optimize the data acquisition process. For example, it is critical to fine-tune the hit rate to maximize the usage of collected data; it is also important to know the current diffraction limit, crystalline mosaicity, reciprocal space coverage, and other relevant factors over time. Therefore, hit finding alone is insufficient to provide the necessary insights, making real-time Bragg peak finding crucial in delivering fast and comprehensive feedback. The previously mentioned peak finder in Psocake runs at roughly 5 Hz on a data center CPU, which may result in substantial cost when attempting to scale up the process.

In this work, we present PeakNet that addresses the problem of high data rate peak finding by converting it into the task of peak segmentation using neural networks. To accomplish this goal, we propose to train a neural network model to classify each individual pixel as either belonging to a peak or not belonging to a peak. This is followed by converting a connected area of pixels as a single peak, a task that can be readily accomplished through connected component

analysis [Weaver, 1985]. Subsequently, the peak coordinates will be determined by computing the center of mass of all the pixels that belong to the identified peak. It is worth noting that the entire peak finding process takes place on GPUs, offering a fully parallelizable approach for achieving scalability. Concretely, our contributions can be summarized as follows:

- We introduce a deep neural network-based Bragg peak finder, named PeakNet, which can effectively and efficiently segment hundreds or even thousands of Bragg peaks with various peak profiles in detector images of any dimension. Despite being trained on peaks labeled by an existing peak finder, we highlight that PeakNet’s capability is not limited by the peak finder used in labeling.
- We demonstrate the efficacy of PeakNet by evaluating its performance on large multi-panel ( $1739 \times 1748$ ) and single-panel ( $1920 \times 1920$ ) detectors. It significantly outperformed existing methods in terms of indexing rate, while delivering comparable number of indexed events. We also fine-tuned the underlying U-Net architecture of PeakNet to strike an optimal balance between model efficacy and runtime performance, leading to a four times out-of-the-box processing speed improvement over Psocake peak finder.

## II. RELATED WORK

Reliable and automatic peak finding algorithms have undergone multiple iterations of development. An early approach involved utilizing template matching [Wilkinson et al., 1988] based on libraries of peak shapes, but this method was found to be slow and inefficient during runtime, especially when dealing with peaks with low signal-to-noise ratios (SNR). The main obstacle lies in the localization of peaks and the tuning of user parameters for pattern matching, compounded by the difficult task of developing a comprehensive library of peak shapes. Another influential approach employed region-growing techniques [Barty et al., 2014, Bolotovskiy et al., 1995] to detect pixel areas with high skewness. In the context of serial crystallography with XFEL sources, the efficacy of this method was diminished due to the lack of sufficient data to provide reliable statistics, rendering it susceptible to outliers and less adept in analyzing weak peaks at higher scattering angles, which are essential for achieving atomic resolution in structure determination.

While template matching and region-growing techniques require users to provide prior information like threshold values, Robust Peak Finder (RPF) [Hadian-Jazi et al., 2017, 2021] has demonstrated proficient peak finding capabilities with minimal user input. This technique utilizes the Modified Selective Statistical Estimator (MSSE) method to segment between background pixels and actual peaks. Furthermore, the RPF method can also parallelize the processing of diffraction patterns, making it suitable for real-time data analysis.

Psocake is a software specifically designed to streamline high throughput data reduction and analysis of XFEL exper-

iments, and is routinely used at SLAC National Accelerator Laboratory (SLAC) and Pohang Accelerator Laboratory (PAL). The built-in peak-finding algorithm [Shin et al., 2018] includes calibrating raw analog-to-digital units (ADUs); applying optional background correction and bad pixel masks; identifying possible peaks; calculating their SNR; determining Bragg spot sizes; and selecting peaks based on size, total intensity and SNR.

In recent years, neural network models have emerged as a promising avenue for Bragg peak finding. BraggNet [Sullivan et al., 2019] is the first method that demonstrates proficiency of neural network models, specifically U-Net [Ronneberger et al., 2015], in accurately segmenting peak pixels, including weak peaks, from background pixels in neutron crystallography data. Specifically, BraggNet employed simulated peaks to create training datasets, which underwent a number of preprocessing steps, including centering and cropping to a specific size and adding Poisson noise. It should be noted that BraggNet works on a single peak at a time within a small 32 by 32 window, which deviates significantly from conventional Bragg peak finding tasks that require extracting peak positions from images typically with hundreds or thousands of pixels along one dimension. Furthermore, another neural network method for Bragg peak analysis was detailed in the work of BraggNN [Liu et al., 2021], emphasizing the refinement of Bragg peak positions without the need for explicit fitting of a profile function, such as the pseudo-Voigt profile. Likewise, BraggNN works on a single peak at a time within a 11 by 11 window, performing regression to two variables representing the peak position. To the best of our knowledge, no existing neural network based peak-finding models have demonstrated the ability to detect multiple peaks with high precision without manual tuning of peak finding parameters, which is the primary goal we strive to achieve with PeakNet.

## III. METHODS

PeakNet uses a U-Net architecture to perform peak segmentation on diffraction images, generating a heatmap of probabilities of a given pixel belonging to a true peak. A probability threshold is subsequently employed to translate the heatmap into a binary mask or segmentation map, with a value of one indicating a peak pixel and zero otherwise. A connected component analysis [Weaver, 1985] is then applied to extract peak positions in image coordinates. The entire peak finding process is summarized in Fig. 1. In this section, we present the details in model training, comprising the specific U-Net architecture, the loss function and the data labeling process.

### A. The segmentation model: U-Net

Peak segmentation in PeakNet is achieved by the use of U-Net [Ronneberger et al., 2015] with a reduced number of feature channels applied in both the contracting and expanding paths, as depicted in Fig. 2. A single contracting layer contains two stride-one and zero-padding  $3 \times 3$  convolutional layers with a rectified linear unit (ReLU) [Fukushima, 1975] and an additional stride-two  $2 \times 2$  max-pooling layer. The number

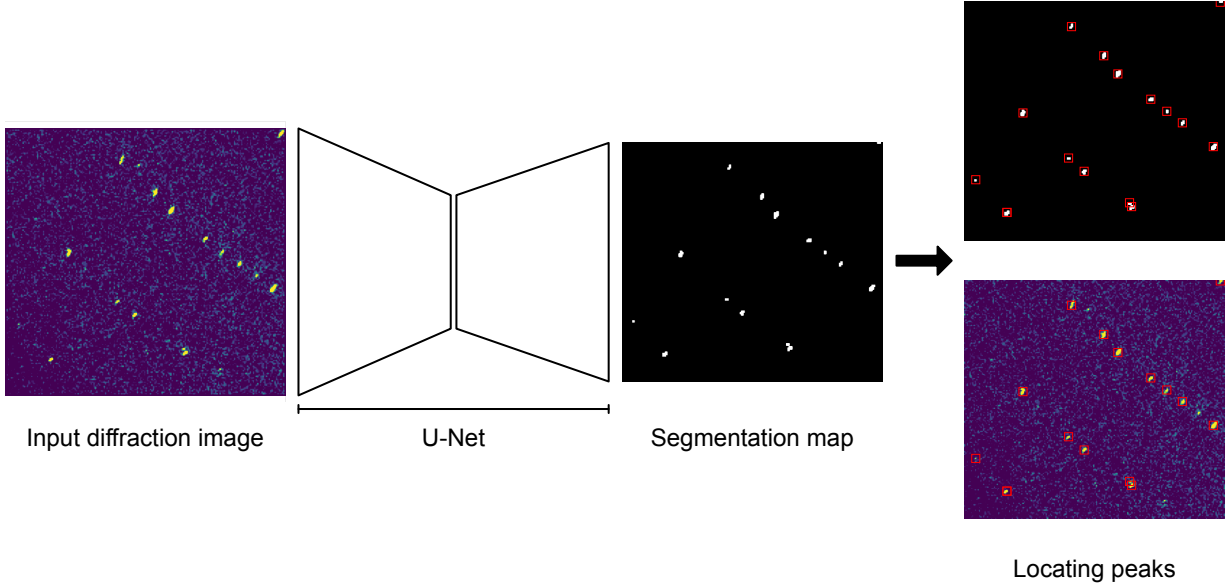


Fig. 1. Peak finding process in PeakNet.

of feature channels doubles with respect to its previous contracting layer. Likewise, a single expanding path contains a stride-two  $2 \times 2$  transposed convolutional layers concatenated with the corresponding feature map from the contracting path. This is followed by two stride-one  $3 \times 3$  convolutional layers connected to a ReLU activation function. It is worth noting that the feature map cropping may be necessary during the concatenation between feature maps from two paths. In the last layer, all 8 channels will be mapped to a single channel through a  $1 \times 1$  convolution.

#### B. The loss function: focal loss

A main technical issue in training U-Net for Bragg peak detection is the extreme peak-background class imbalance (e.g.,  $> 10^3 : 1$ ), resulting in reduced prediction accuracy. This may not pose as a problem in previous peak finders like BraggNet, which operates on a much smaller area of  $32 \times 32$ , whereas PeakNet is trained on larger multi-panel detectors, such as the Cornell-SLAC pixel array detector (CSPAD) [Hart et al., 2012] with a dimension of  $194 \times 185$  for one of its panels. Focal loss was introduced to address the extreme class imbalance problem for object detectors [Lin et al., 2018]. It is defined as:

$$FL(p) = -\alpha \cdot (1-p)^\gamma \cdot \log p. \quad (1)$$

Here,  $p$  is the probabilities of a pixel  $x$  being a peak.  $\gamma$  controls a modulating factor  $(1-p)$  and  $\alpha$  is an additional modulating factor. We used  $\gamma = 2.0$  and  $\alpha = 1.2$  in PeakNet. In practice, numerical instability will often emerge in the calculation of  $p = e^{-\text{logit}}$ , where  $\text{logit} = \log(1 + e^{-x})$ . To bypass this issue, logit needs to be rewritten as  $\text{logit} =$

$a + \log(e^{-a} + e^{-x-a})$ , where  $a = \max(0, -x)$ . As a result, if we denote the label of a pixel  $x$  as  $y$ , the focal loss becomes

$$FL(p) = \alpha \cdot y \cdot (1-p)^\gamma + \text{logit} + (1-y) \cdot p^\gamma \cdot x + p^\gamma \cdot (1-y) \cdot \text{logit} \quad (2)$$

## IV. EXPERIMENTS

### A. PeakNet on multi-panel detectors: Trained on panels but predicting on assembled images.

We demonstrated the possibility of PeakNet making prediction on assembled images from a multi-panel detector despite being trained on individual panels. To facilitate this investigation, we utilized a multi-panel detector CSPAD, which is widely used in serial crystallography experiments at LCLS. Specifically, we used crystallographic data of streptavidin crystals from LCLS experiment *cxic0415* run *101* at the Coherent X-ray Imaging (CXI) instrument, where the CSPAD deployed consists of 32 panels. An individual diffraction image recorded on CSPAD are conventionally saved in a stack of 64 mini-panels (half of a physical CSPAD panel). For data labeling, we randomly selected 268 mini-panels, which were labeled using the Psocake peak finder with the default settings. We then split the labeled data into 60% training set and 20% validation set. The remaining 20% data were initially set aside for testing purposes, but were not used due to the lack of an effective metric, which will be discussed later in the evaluation of our model's efficacy. Our test set included the first 5000 events of the run, which facilitated a faster feedback loop compared with going through all events in the run. Notably, we did not apply any image preprocessing, and thus PeakNet

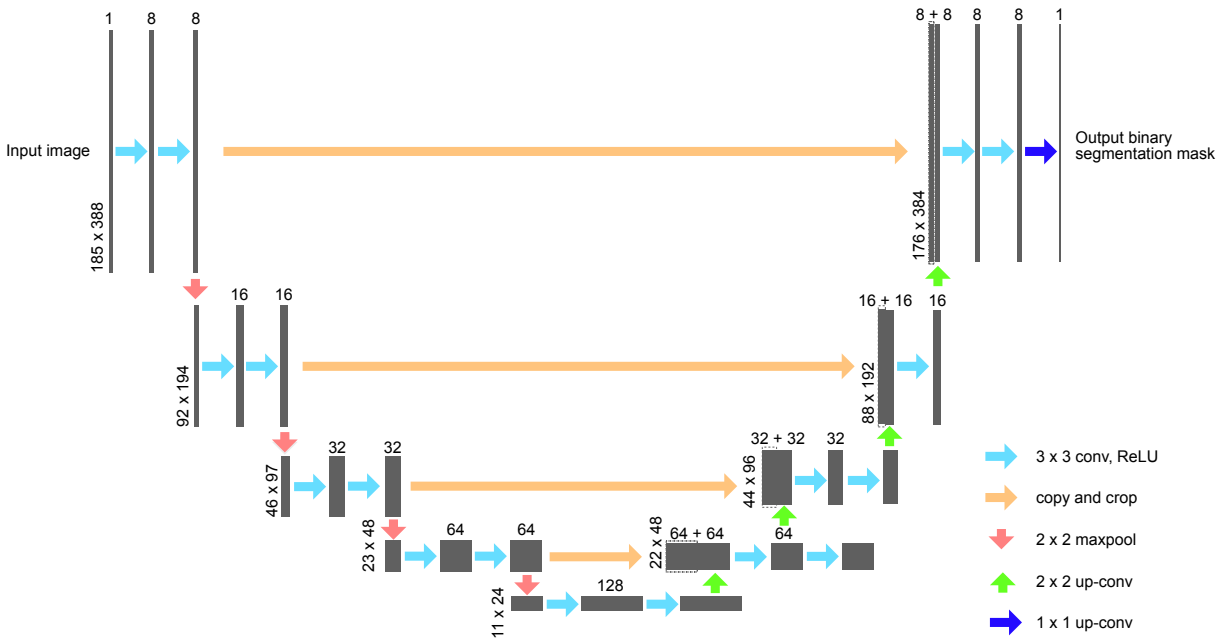


Fig. 2. The U-Net architecture in PeakNet.

directly takes in a diffraction image of its original size and outputs a segmentation map.

Fig. 3 (a) displays labeled samples, with the input mini-panel image on the left and pixel-wise labeled peaks on the right. The overall peak label is a binary mask that shares the same size as the input, with a value of one indicating a peak pixel and zero otherwise. Consequently, each input consists of a  $185 \times 194$  mini-panel from the CSPAD and a binary mask of the same size. Additionally, Fig. 3 (b) shows a sample model prediction on an entire CSPAD image with a size of  $1739 \times 1748$ .

### B. Examining PeakNet’s generalizability beyond the peak finder used in labeling

The current strategy for data labeling involves using an existing peak finder, and it is important to evaluate whether any limitations of the peak finder used in data labeling will affect the peak finding capability of PeakNet. One specific limitation to investigate is the size dependency of the peak finder. Notably, the peak size range is a user-defined input requested by the Psocake peak finder. This works well when diffraction spots have consistent sizes. However, detectors such as the Rayonix have a large point spread function for intense peaks, which may result in large peaks being ignored by the Psocake peak finder. Consequently, there is a concern about whether PeakNet will inherit the same limitations since it is trained on Psocake peak labels.

Fig. 4 presents a side-by-side comparison of peak detection on a Rayonix image, with the PeakNet results displayed on the left and the Psocake results on the right. The diffraction data were collected from crystals of SARS-CoV-2 proteases using the Macromolecular Femtosecond Crystallography (MFX) in-

strument [Sierra et al., 2019] at LCLS. Upon visual inspection of Fig. 4 (c) and (d), both PeakNet and Psocake were observed to detect a considerable number of peaks, suggesting a potentially comparable performance between the two methods. However, upon closer inspection of the view near the area slightly below the beamstop position, one obvious, reasonably sized Bragg peak was observed but not detected by the Psocake peak finder, whereas PeakNet successfully located this peak. This finding provides direct evidence that PeakNet’s peak finding capability is not strictly limited by the peak finder used in the data labeling process. In fact, PeakNet appears to possess its own understanding of Bragg peaks, as evidenced by the exclusion of a weak single Bragg peak-like spot near the upper edge of the image, as shown in Fig. 4 (a) and (b). Therefore, it is important to note that PeakNet is not merely a neural network-based replica of the Psocake peak finder despite being trained on labels supplied by it.

### C. Model efficacy and runtime performance

We consider model efficacy of a peak finder in two metrics: (1) indexing rate and (2) the number of indexed events. Table I provides a comparative analysis of two distinct datasets, CXI and MFX, showcasing the outcomes obtained when processed using two peak finders, Psocake and PeakNet. The detectors employed for the respective datasets are CSPAD and Rayonix. The analyzed events for the CXI dataset span from 0 to 5000, whereas the MFX dataset encompasses a range of 0 to 8998. Psocake identified 2107 events in the CXI dataset and 465 in the MFX dataset, yielding indexing rates of 71.2% and 84.5%, respectively. In contrast, PeakNet discovered 1991 events in the CXI dataset and 430 in the MFX dataset, exhibiting superior indexing rates of 78.6%

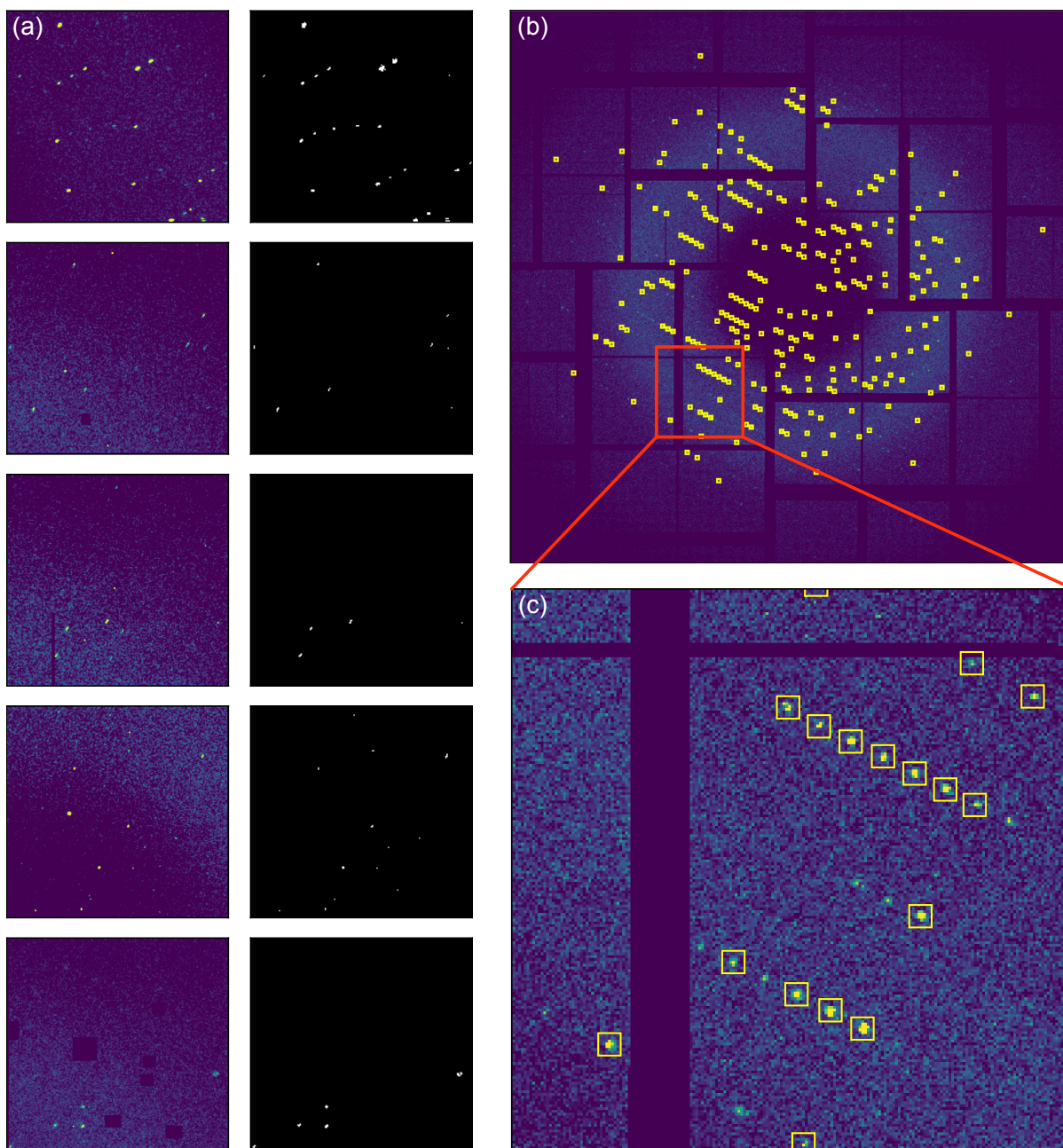


Fig. 3. (a) PeakNet input images and peak labels. (b) PeakNet prediction on an entire CSPAD image. (c) A magnified view of a small region of the detector.

and 90.2%, respectively. Although both peak finders exhibit varying levels of effectiveness, our evaluation has revealed that PeakNet achieves superior indexing rates across both datasets, while also yielding comparable numbers of indexed events. These results suggest that PeakNet may represent a more reliable and efficient solution for the analysis of such data.

To provide further context and justification for this efficacy measure, it is important to note that conventional metrics like accuracy, precision and F-1 scores are not always well-defined in the context of peak finding, due to the lack of actual “ground truth”. This is because the peak labels used

for training and evaluation are derived from another peak finder, rather than being uniquely determined in some fashion. As a result, it is necessary to consider alternative measures of model performance and reliability, such as the indexing rate and the number of indexed events. However, conventional metrics may remain a viable option when applied to synthetic data generated by a simulator. For clarification purposes, we used the *indexamajig* tool within the *CrystFEL* data analysis software [White et al., 2012] to perform indexing. We employed multiple indexing methods, including *mosflm*, *xds* and *xgandalf*, with an additional setting of *-int-radius=4,5,6*.

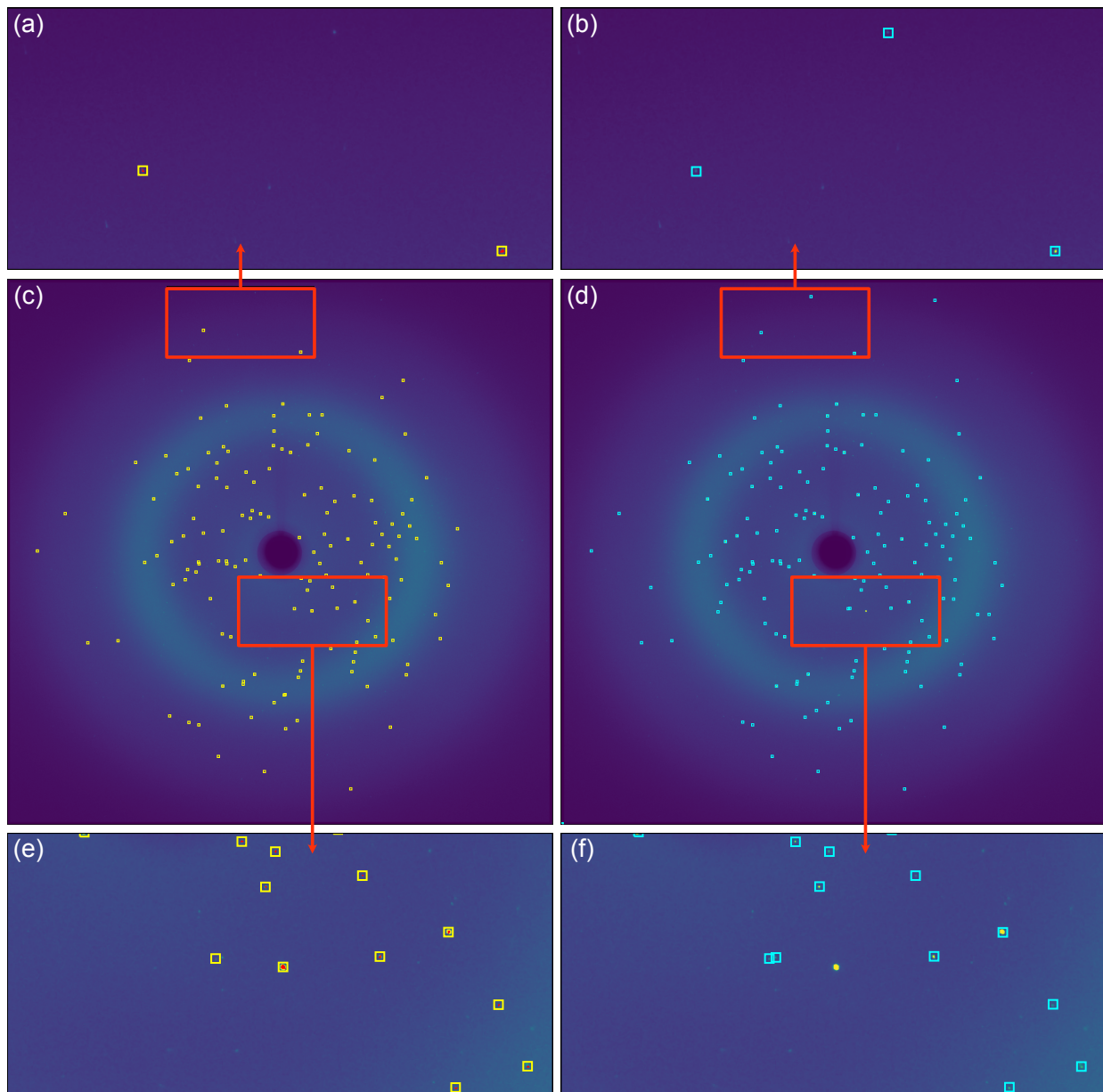


Fig. 4. Peak finding on a Rayonix image using (c) PeakNet and (d) Psocake. (a), (b), (c) and (d) are magnified views of some regions.

TABLE I  
PEAK FINDING AND INDEXING RESULTS.

Dataset	CXI	MFX
Detector	CSPAD	Rayonix
Events to analyze	0-5000	0-8998
Psocake: Hits found	2107	465
Psocake: Indexed	1501	393
Psocake: Indexing rate	71.2%	84.5%
PeakNet: Hits found	1991	430
PeakNet: Indexed	1565	388
PeakNet: Indexing rate	78.6%	90.2%

Furthermore, while the runtime performance of PeakNet is excellent as compared with other crystallography data analysis methods in Table II, there is a caveat to consider. Although

PeakNet is designed as a nearly end-to-end solution, with its neural networks returning a segmentation map that represents the pixel-wise probability of being a peak from input diffraction images, we must employ connected component analysis to convert the segmentation maps into peak coordinates. While the neural network runtime is exceptionally fast, capable of processing 11 Rayonix images ( $1920 \times 1920$ ) in parallel on a 1080 Ti GPU in just 4ms (equivalent to 0.36 ms per image), the additional time required for connected component analysis is considerably longer and thus a significant runtime bottleneck in the current version of PeakNet. In fact, this bottleneck processing time scales nearly linearly with respect to the number of images, and it adds an additional 30ms of processing time for each image despite running on the same

GPU. Practically speaking, the current version of PeakNet runs at 49ms per Rayonix event on 1080 Ti, which is actually 10 × faster than some diffraction image classification algorithms.

## V. CONCLUSIONS

In this paper, we introduced PeakNet, a deep learning-based peak finder that efficiently tackles the Bragg peak finding problem as a semantic segmentation task. The U-Net architecture of PeakNet has been optimized to achieve an ideal balance between efficacy and runtime performance, resulting in a processing speed four times faster than the Psocake peak finder while maintaining superior indexing rates and a comparable number of indexed events. A notable bottleneck in the current version of PeakNet is the connected component analysis, which scales linearly with input data volume, whereas the neural network portion scales beyond linear capability on GPUs, limited largely by GPU memory. It is worth mentioning that the current data reduction concept primarily focuses on processing single events as quickly as possible, centering the design principle on CPUs. However, with neural networks, we propose a new direction towards batch image processing on GPUs, exemplified by PeakNet in the context of serial crystallography.

## ACKNOWLEDGMENT

Earlier versions of the U-Net models were built and tested by P.L. under the supervision of C.H.Y. The experiments were designed by C.W. with inputs from J.B.T. and C.H.Y. C.W. prepared the datasets, labeled experimental data, and trained and evaluated the refined neural network model. The manuscript was written by C.W. and C.H.Y. with input from all authors. This material is based upon work supported by the U.S. Department of Energy, Office of Science, Office of Basic Energy Sciences under Award Number FWP-100643. Use of the Linac Coherent Light Source (LCLS), SLAC National Accelerator Laboratory, is supported by the U.S. Department of Energy, Office of Science, Office of Basic Energy Sciences under Contract No. DE-AC02-76SF00515.

## REFERENCES

Aschkan Allahgholi, Julian Becker, Annette Delfs, Roberto Dinapoli, Peter Goettlicher, Dominic Greiffenberg, Beat Henrich, Helmut Hirsemann, Manuela Kuhn, Robert Klanner, Alexander Klyuev, Hans Krueger, Sabine Lange, Torsten Laurus, Alessandro Marras, Davide Mezza, Aldo Mozzanica, Magdalena Niemann, Jennifer Poehlsen, Joern Schwandt, Igor Sheviakov, Xintian Shi, Sergej Smoljanin, Lothar Steffen, Jolanta Sztuk-Dambietz, Ulrich Trunk, Qingqing Xia, Mourad Zeribi, Jianguo Zhang, Manfred Zimmer, Bernd Schmitt, and Heinz Graafsma. The Adaptive Gain Integrating Pixel Detector at the European XFEL. *Journal of Synchrotron Radiation*, 26(1):74–82, January 2019. ISSN 1600-5775. doi: 10.1107/S1600577518016077.

Andrew Aquila, Mark S. Hunter, R. Bruce Doak, Richard A. Kirian, Petra Fromme, Thomas A. White, Jakob Andreasson, David Arnlund, Saša Bajt, Thomas R. M. Barends,

Miriam Barthelmess, Michael J. Bogan, Christoph Bostedt, Hervé Bottin, John D. Bozek, Carl Caleman, Nicola Coppola, Jan Davidsson, Daniel P. DePonte, Veit Elser, Sascha W. Epp, Benjamin Erk, Holger Fleckenstein, Lutz Foucar, Matthias Frank, Raimund Fromme, Heinz Graafsma, Ingo Grotjohann, Lars Gumprecht, Janos Hajdu, Christina Y. Hampton, Andreas Hartmann, Robert Hartmann, Stefan Hau-Riege, Günter Hauser, Helmut Hirsemann, Peter Holl, James M. Holton, André Hömke, Linda Johansson, Nils Kimmel, Stephan Kassemeyer, Faton Krasniqi, Kai-Uwe Kühnel, Mengning Liang, Lukas Lomb, Erik Malmerberg, Stefano Marchesini, Andrew V. Martin, Filipe R.N.C. Maia, Marc Messerschmidt, Karol Nass, Christian Reich, Richard Neutze, Daniel Rolles, Benedikt Rudek, Artem Rudenko, Ilme Schlichting, Carlo Schmidt, Kevin E. Schmidt, Joachim Schulz, M. Marvin Seibert, Robert L. Shoeman, Raymond Sierra, Heike Soltau, Dmitri Starodub, Francesco Stellato, Stephan Stern, Lothar Strüder, Nicusor Timneanu, Joachim Ullrich, Xiaoyu Wang, Garth J. Williams, Georg Weidenspointner, Uwe Weierstall, Cornelia Wunderer, Anton Barty, John C. H. Spence, and Henry N. Chapman. Time-resolved protein nanocrystallography using an X-ray free-electron laser. *Optics Express*, 20(3):2706, January 2012. ISSN 1094-4087. doi: 10.1364/OE.20.002706.

Anton Barty, Richard A. Kirian, Filipe R. N. C. Maia, Max Hantke, Chun Hong Yoon, Thomas A. White, and Henry Chapman. *Cheetah*: Software for high-throughput reduction and analysis of serial femtosecond X-ray diffraction data. *Journal of Applied Crystallography*, 47(3):1118–1131, June 2014. ISSN 1600-5767. doi: 10.1107/S1600576714007626.

R. Bolotovskiy, M. A. White, A. Darovsky, and P. Coppens. The ‘Seed-Skewness’ Method for Integration of Peaks on Imaging Plates. *Journal of Applied Crystallography*, 28(2):86–95, April 1995. ISSN 0021-8898. doi: 10.1107/S0021889894009696.

Henry N. Chapman, Anton Barty, Michael J. Bogan, Sébastien Boutet, Matthias Frank, Stefan P. Hau-Riege, Stefano Marchesini, Bruce W. Woods, Saša Bajt, W. Henry Benner, Richard A. London, Elke Plönjes, Marion Kuhlmann, Rolf Treusch, Stefan Düsterer, Thomas Tschentscher, Jochen R. Schneider, Eberhard Spiller, Thomas Möller, Christoph Bostedt, Matthias Hoener, David A. Shapiro, Keith O. Hodgson, David van der Spoel, Florian Burmeister, Magnus Bergh, Carl Caleman, Gösta Huldt, M. Marvin Seibert, Filipe R. N. C. Maia, Richard W. Lee, Abraham Szöke, Nicusor Timneanu, and Janos Hajdu. Femtosecond diffractive imaging with a soft-X-ray free-electron laser. *Nature Physics*, 2(12):839–843, December 2006. ISSN 1745-2473, 1745-2481. doi: 10.1038/nphys461.

Henry N. Chapman, Petra Fromme, Anton Barty, Thomas A. White, Richard A. Kirian, Andrew Aquila, Mark S. Hunter, Joachim Schulz, Daniel P. DePonte, Uwe Weierstall, R. Bruce Doak, Filipe R. N. C. Maia, Andrew V. Martin, Ilme Schlichting, Lukas Lomb, Nicola Coppola, Robert L. Shoeman, Sascha W. Epp, Robert Hartmann,

TABLE II

THE RUNTIME PERFORMANCE OF DIFFRACTION IMAGE ANALYSIS ALGORITHMS MEASURED ON RAYONIX IMAGES CONTAINING 3.7 MEGAPIXELS. WE MEASURED RUNTIME PERFORMANCE OF PSOCAKE AND PEAKNET DIRECTLY USING RAYONIX IMAGES. FOR REFERENCE PURPOSES, WE ALSO INCLUDED ANOTHER PEAK FINDING METHOD RPF [HADIAN-JAZI ET AL., 2017, 2021] AND TWO CLASSIFICATION METHODS FOR X-RAY DIFFRACTION DATA REDUCTION. RPF RUNTIME PERFORMANCE WAS ORIGINALLY MEASURED ON AGIPD 1M [ALLAHHOLI ET AL., 2019]. THE TWO CLASSIFICATION METHODS WERE EVALUATED ON 0.5 MEGAPIXEL IMAGES USING THE CNN HIT FINDER METHOD [KE ET AL., 2018], WHICH WAS ALSO USED AS A POINT OF COMPARISON IN THE ORB+MLP METHOD [RAHMANI ET AL., 2023]. A \* NOTATION WAS USED TO INDICATE A LINEARLY EXTRAPOLATED PROCESSING TIME, BUT THE REAL PERFORMANCE MAY VARY DEPENDING ON THE SPECIFIC HARDWARE AND THE COMPLEXITY OF THE UNDERLYING ALGORITHM.

Method	Task	Hardware	Image size	Time (ms/event)
RPF	Peak Finding	Intel E5-2698	1024 × 1024	~120.0
			1920 × 1920	~421.8*
Psocake	Peak Finding	Intel E5-2620	1920 × 1920	200.0
<b>PeakNet</b>	Peak Finding	NVIDIA 1080 Ti	1920 × 1920	<b>49.0</b>
CNN hit finder	Classification	NVIDIA 1080 Ti	720 × 720	0.8
			1920 × 1920	5.6*
ORB+MLP	Classification	Intel Core i5	720 × 720	50.0
			1920 × 1920	355.6*

- Daniel Rolles, Artem Rudenko, Lutz Foucar, Nils Kimmel, Georg Weidenspointner, Peter Holl, Mengning Liang, Miriam Barthelmess, Carl Caleman, Sébastien Boutet, Michael J. Bogan, Jacek Krzywinski, Christoph Bostedt, Saša Bajt, Lars Gumprecht, Benedikt Rudek, Benjamin Erk, Carlo Schmidt, André Hömke, Christian Reich, Daniel Pietschner, Lothar Strüder, Günter Hauser, Hubert Gorke, Joachim Ullrich, Sven Herrmann, Gerhard Schaller, Florian Schopper, Heike Soltau, Kai-Uwe Kühnel, Marc Messerschmidt, John D. Bozek, Stefan P. Hau-Riege, Matthias Frank, Christina Y. Hampton, Raymond G. Sierra, Dmitri Starodub, Garth J. Williams, Janos Hajdu, Nicusor Timneanu, M. Marvin Seibert, Jakob Andreasson, Andrea Rocker, Olof Jönsson, Martin Svenda, Stephan Stern, Karol Nass, Robert Andritschke, Claus-Dieter Schröter, Faton Krasniqi, Mario Bott, Kevin E. Schmidt, Xiaoyu Wang, Ingo Grotjohann, James M. Holton, Thomas R. M. Barends, Richard Neutze, Stefano Marchesini, Raimund Fromme, Sebastian Schorb, Daniela Rupp, Marcus Adolph, Tais Gorkhover, Inger Andersson, Helmut Hirsemann, Guillaume Potdevin, Heinz Graafsma, Björn Nilsson, and John C. H. Spence. Femtosecond X-ray protein nanocrystallography. *Nature*, 470(7332):73–77, February 2011. ISSN 0028-0836, 1476-4687. doi: 10.1038/nature09750.
- Kunihiko Fukushima. Cognitron: A self-organizing multilayered neural network. *Biological Cybernetics*, 20(3-4):121–136, 1975. ISSN 0340-1200, 1432-0770. doi: 10.1007/BF00342633.
- Marjan Hadian-Jazi, Marc Messerschmidt, Connie Darmanin, Klaus Giewekemeyer, Adrian P. Mancuso, and Brian Abbey. A peak-finding algorithm based on robust statistical analysis in serial crystallography. *Journal of Applied Crystallography*, 50(6):1705–1715, December 2017. ISSN 1600-5767. doi: 10.1107/S1600576717014340.
- Marjan Hadian-Jazi, Alireza Sadri, Anton Barty, Oleksandr Yefanov, Marina Galchenkova, Dominik Oberthuer, Dana Komadina, Wolfgang Brehm, Henry Kirkwood, Grant Mills, Raphael de Wijn, Romain Letrun, Marco Kloos, Mohammad Vakili, Luca Gelisio, Connie Darmanin, Adrian P. Mancuso, Henry N. Chapman, and Brian Abbey. Data reduction for serial crystallography using a robust peak finder. *Journal of Applied Crystallography*, 54(5):1360–1378, October 2021. ISSN 1600-5767. doi: 10.1107/S1600576721007317.
- P. Hart, S. Boutet, G. Carini, A. Dragone, B. Duda, D. Freytag, G. Haller, R. Herbst, S. Herrmann, C. Kenney, J. Morse, M. Nordby, J. Pines, N. van Bakel, M. Weaver, and G. Williams. The Cornell-SLAC pixel array detector at LCLS. In *2012 IEEE Nuclear Science Symposium and Medical Imaging Conference Record (NSS/MIC)*, pages 538–541, Anaheim, CA, USA, October 2012. IEEE. ISBN 978-1-4673-2030-6 978-1-4673-2028-3 978-1-4673-2029-0. doi: 10.1109/NSSMIC.2012.6551166.
- Mohamed Ibrahim, Thomas Fransson, Ruchira Chatterjee, Mun Hon Cheah, Rana Hussein, Louise Lassalle, Kyle D. Sutherland, Iris D. Young, Franklin D. Fuller, Sheraz Gul, In-Sik Kim, Philipp S. Simon, Casper de Lightenberg, Petko Chernev, Isabel Bogacz, Cindy C. Pham, Allen M. Orville, Nicholas Saichek, Trent Northen, Alexander Batyuk, Sergio Carbajo, Roberto Alonso-Mori, Kensuke Tono, Shigeki Owada, Asmit Bhowmick, Robert Bolotovskiy, Derek Mendez, Nigel W. Moriarty, James M. Holton, Holger Dobbek, Aaron S. Brewster, Paul D. Adams, Nicholas K. Sauter, Uwe Bergmann, Athina Zouni, Johannes Messinger, Jan Kern, Vittal K. Yachandra, and Junko Yano. Untangling the sequence of events during the  $S_2 \rightarrow S_3$  transition in photosystem II and implications for the water oxidation mechanism. *Proceedings of the National Academy of Sciences*, 117(23):12624–12635, June 2020. ISSN 0027-8424, 1091-6490. doi: 10.1073/pnas.2000529117.
- Tsung-Wei Ke, Aaron S. Brewster, Stella X. Yu, Daniela Ushizima, Chao Yang, and Nicholas K. Sauter. A convolutional neural network-based screening tool for X-ray serial crystallography. *Journal of Synchrotron Radiation*, 25(3):655–670, May 2018. ISSN 1600-5775. doi: 10.1107/S1600577518004873.
- Jan Kern, Ruchira Chatterjee, Iris D. Young, Franklin D. Fuller, Louise Lassalle, Mohamed Ibrahim, Sheraz Gul, Thomas Fransson, Aaron S. Brewster, Roberto Alonso-



- Mori, Rana Hussein, Miao Zhang, Lacey Douthit, Casper de Lichtenberg, Mun Hon Cheah, Dmitry Shevela, Julia Wersig, Ina Seuffert, Dimosthenis Sokaras, Ernest Pastor, Clemens Weninger, Thomas Kroll, Raymond G. Sierra, Pierre Aller, Agata Butryn, Allen M. Orville, Mengning Liang, Alexander Batyuk, Jason E. Koglin, Sergio Carbajo, Sébastien Boutet, Nigel W. Moriarty, James M. Holton, Holger Dobbek, Paul D. Adams, Uwe Bergmann, Nicholas K. Sauter, Athina Zouni, Johannes Messinger, Junko Yano, and Vittal K. Yachandra. Structures of the intermediates of Kok's photosynthetic water oxidation clock. *Nature*, 563(7731):421–425, November 2018. ISSN 0028-0836, 1476-4687. doi: 10.1038/s41586-018-0681-2.
- Christopher Kupitz, Shibom Basu, Ingo Grotjohann, Raimund Fromme, Nadia A. Zatsepin, Kimberly N. Rendek, Mark S. Hunter, Robert L. Shoeman, Thomas A. White, Dingjie Wang, Daniel James, Jay-How Yang, Danielle E. Cobb, Brenda Reeder, Raymond G. Sierra, Haiguang Liu, Anton Barty, Andrew L. Aquila, Daniel Deponte, Richard A. Kirian, Sadia Bari, Jesse J. Bergkamp, Kenneth R. Beylerlein, Michael J. Bogan, Carl Caleman, Tzu-Chiao Chao, Chelsie E. Conrad, Katherine M. Davis, Holger Fleckenstein, Lorenzo Galli, Stefan P. Hau-Riege, Stephan Kasse-meyer, Hartawan Laksmono, Mengning Liang, Lukas Lomb, Stefano Marchesini, Andrew V. Martin, Marc Messerschmidt, Despina Milathianaki, Karol Nass, Alexandra Ros, Shatabdi Roy-Chowdhury, Kevin Schmidt, Marvin Seibert, Jan Steinbrener, Francesco Stellato, Lifan Yan, Chunhong Yoon, Thomas A. Moore, Ana L. Moore, Yulia Pushkar, Garth J. Williams, Sébastien Boutet, R. Bruce Doak, Uwe Weierstall, Matthias Frank, Henry N. Chapman, John C. H. Spence, and Petra Fromme. Serial time-resolved crystallography of photosystem II using a femtosecond X-ray laser. *Nature*, 513(7517):261–265, September 2014. ISSN 0028-0836, 1476-4687. doi: 10.1038/nature13453.
- Tsung-Yi Lin, Priya Goyal, Ross Girshick, Kaiming He, and Piotr Dollár. Focal Loss for Dense Object Detection, February 2018.
- Zhengchun Liu, Hemant Sharma, Jun-Sang Park, Peter Kene-sei, Antonino Miceli, Jonathan Almer, Rajkumar Ket-timuthu, and Ian Foster. BraggNN: Fast X-ray Bragg Peak Analysis Using Deep Learning. *arXiv:2008.08198 [cs, eess]*, June 2021.
- Eriko Nango, Antoine Royant, Minoru Kubo, Takanori Nakane, Cecilia Wickstrand, Tetsunari Kimura, Tomoyuki Tanaka, Kensuke Tono, Changyong Song, Rie Tanaka, Toshi Arima, Ayumi Yamashita, Jun Kobayashi, Toshi-aki Hosaka, Eiichi Mizohata, Przemyslaw Nogly, Michi-hiro Sugahara, Daewoong Nam, Takashi Nomura, Tatsuro Shimamura, Dohyun Im, Takaaki Fujiwara, Yasuaki Ya-manaka, Byeonghyun Jeon, Tomohiro Nishizawa, Kazu-masa Oda, Masahiro Fukuda, Rebecka Andersson, Petra Båth, Robert Dods, Jan Davidsson, Shigeru Matsuoka, Satoshi Kawatake, Michio Murata, Osamu Nureki, Shigeki Owada, Takashi Kameshima, Takaki Hatsui, Yasumasa Joti, Gebhard Schertler, Makina Yabashi, Ana-Nicoleta Bon-dar, Jörg Standfuss, Richard Neutze, and So Iwata. A three-dimensional movie of structural changes in bacteriorhodopsin. *Science*, 354(6319):1552–1557, December 2016. ISSN 0036-8075, 1095-9203. doi: 10.1126/science.aah3497.
- Richard Neutze, Remco Wouts, David van der Spoel, Edgar Weckert, and Janos Hajdu. Potential for biomolecular imaging with femtosecond X-ray pulses. *Nature*, 406(6797):752–757, August 2000. ISSN 0028-0836, 1476-4687. doi: 10.1038/35021099.
- Kanupriya Pande, Christopher D. M. Hutchison, Gerrit Groen-hof, Andy Aquila, Josef S. Robinson, Jason Tenboer, Shi-bom Basu, Sébastien Boutet, Daniel P. DePonte, Mengning Liang, Thomas A. White, Nadia A. Zatsepin, Oleksandr Yefanov, Dmitry Morozov, Dominik Oberthuer, Cornelius Gati, Ganesh Subramanian, Daniel James, Yun Zhao, Jake Koralek, Jennifer Brayshaw, Christopher Kupitz, Chelsie Conrad, Shatabdi Roy-Chowdhury, Jesse D. Coe, Markus Metz, Paulraj Lourdu Xavier, Thomas D. Grant, Jason E. Koglin, Gihan Ketawala, Raimund Fromme, Vukica Šrajer, Robert Henning, John C. H. Spence, Abbas Ourmazd, Peter Schwander, Uwe Weierstall, Matthias Frank, Petra Fromme, Anton Barty, Henry N. Chapman, Keith Moffat, Jasper J. van Thor, and Marius Schmidt. Femtosecond structural dynamics drives the trans/cis isomerization in photoactive yellow protein. *Science*, 352(6286):725–729, May 2016. ISSN 0036-8075, 1095-9203. doi: 10.1126/science.aad5081.
- Vahid Rahmani, Shah Nawaz, David Pennicard, Shabarish Pala Ramakantha Setty, and Heinz Graafsma. Data reduction for X-ray serial crystallography using machine learning. *Journal of Applied Crystallography*, 56(1):200–213, February 2023. ISSN 1600-5767. doi: 10.1107/S1600576722011748.
- Olaf Ronneberger, Philipp Fischer, and Thomas Brox. U-Net: Convolutional Networks for Biomedical Image Segmentation. *arXiv:1505.04597 [cs]*, May 2015.
- Hocheol Shin, Seungnam Kim, and Chun Hong Yoon. Data Analysis using Psocake at PAL-XFEL. *Journal of the Korean Physical Society*, 73(1):16–20, July 2018. ISSN 0374-4884, 1976-8524. doi: 10.3938/jkps.73.16.
- Raymond G. Sierra, Alexander Batyuk, Zhibin Sun, Andrew Aquila, Mark S. Hunter, Thomas J. Lane, Mengning Liang, Chun Hong Yoon, Roberto Alonso-Mori, Rebecca Armenta, Jean-Charles Castagna, Michael Hollenbeck, Ted O. Osier, Matt Hayes, Jeff Aldrich, Robin Curtis, Jason E. Koglin, Theodore Rendahl, Evan Rodriguez, Sergio Carbajo, Serge Guillet, Rob Paul, Philip Hart, Kazutaka Nakahara, Gabriella Carini, Hasan DeMirici, E. Han Dao, Brandon M. Hayes, Yashas P. Rao, Matthieu Chollet, Yiping Feng, Franklin D. Fuller, Christopher Kupitz, Takahiro Sato, Matthew H. Seaberg, Sanghoon Song, Tim B. van Driel, Hasan Yavas, Diling Zhu, Aina E. Cohen, Soichi Wakatsuki, and Sébastien Boutet. The Macromolecular Femtosecond Crystallography Instrument at the Linac Coherent Light Source. *Journal of Synchrotron Radiation*, 26(2):346–357, March 2019. ISSN 1600-5775. doi:

10.1107/S1600577519001577.

- Michihiro Suga, Fusamichi Akita, Michihiro Sugahara, Minoru Kubo, Yoshiki Nakajima, Takanori Nakane, Keitaro Yamashita, Yasufumi Umena, Makoto Nakabayashi, Takahiro Yamane, Takamitsu Nakano, Mamoru Suzuki, Tetsuya Masuda, Shigeyuki Inoue, Tetsunari Kimura, Takashi Nomura, Shinichiro Yonekura, Long-Jiang Yu, Tomohiro Sakamoto, Taiki Motomura, Jing-Hua Chen, Yuki Kato, Takumi Noguchi, Kensuke Tono, Yasumasa Joti, Takashi Kameshima, Takaki Hatsui, Eriko Nango, Rie Tanaka, Hisashi Naitow, Yoshinori Matsuura, Ayumi Yamashita, Masaki Yamamoto, Osamu Nureki, Makina Yabashi, Tetsuya Ishikawa, So Iwata, and Jian-Ren Shen. Light-induced structural changes and the site of O=O bond formation in PSII caught by XFEL. *Nature*, 543(7643): 131–135, March 2017. ISSN 0028-0836, 1476-4687. doi: 10.1038/nature21400.
- Michihiro Suga, Atsuhiko Shimada, Fusamichi Akita, Jian-Ren Shen, Takehiko Tosha, and Hiroshi Sugimoto. Time-resolved studies of metalloproteins using X-ray free electron laser radiation at SACLA. *Biochimica et Biophysica Acta (BBA) - General Subjects*, 1864(2):129466, February 2020. ISSN 03044165. doi: 10.1016/j.bbagen.2019.129466.
- Brendan Sullivan, Rick Archibald, Jahaun Azadmanesh, Venu Gopal Vandavasi, Patricia S. Langan, Leighton Coates, Vickie Lynch, and Paul Langan. BraggNet: Integrating Bragg peaks using neural networks. *Journal of Applied Crystallography*, 52(4):854–863, August 2019. ISSN 1600-5767. doi: 10.1107/S1600576719008665.
- James R. Weaver. Centrosymmetric (Cross-Symmetric) Matrices, Their Basic Properties, Eigenvalues, and Eigenvectors. *The American Mathematical Monthly*, 92(10):711, December 1985. ISSN 00029890. doi: 10.2307/2323222.
- Thomas A. White, Richard A. Kirian, Andrew V. Martin, Andrew Aquila, Karol Nass, Anton Barty, and Henry N. Chapman. *CrystFEL*: A software suite for snapshot serial crystallography. *Journal of Applied Crystallography*, 45(2):335–341, April 2012. ISSN 0021-8898. doi: 10.1107/S0021889812002312.
- C. Wilkinson, H. W. Khamis, R. F. D. Stansfield, and G. J. McIntyre. Integration of single-crystal reflections using area multidetectors. *Journal of Applied Crystallography*, 21(5): 471–478, October 1988. ISSN 0021-8898. doi: 10.1107/S0021889888005400.
- Graeme Winter, David G. Waterman, James M. Parkhurst, Aaron S. Brewster, Richard J. Gildea, Markus Gerstel, Luis Fuentes-Montero, Melanie Vollmar, Tara Michels-Clark, Iris D. Young, Nicholas K. Sauter, and Gwyndaf Evans. Dials: implementation and evaluation of a new integration package. *Acta crystallographica. Section D, Structural biology*, 74:85–97, 2018. ISSN 2059-7983. doi: 10.1107/S2059798317017235. URL <https://pubmed.ncbi.nlm.nih.gov/29533234/>.
- Iris D. Young, Mohamed Ibrahim, Ruchira Chatterjee, Sheraz Gul, Franklin D. Fuller, Sergey Koroidov, Aaron S. Brewster, Rosalie Tran, Roberto Alonso-Mori, Thomas Kroll, Tara Michels-Clark, Hartawan Laksmono, Raymond G. Sierra, Claudiu A. Stan, Rana Hussein, Miao Zhang, Lacey Douthit, Markus Kubin, Casper de Lichtenberg, Long Vo Pham, Håkan Nilsson, Mun Hon Cheah, Dmitriy Shevela, Claudio Saracini, Mackenzie A. Bean, Ina Seuffert, Dimosthenis Sokaras, Tsu-Chien Weng, Ernest Pastor, Clemens Weninger, Thomas Fransson, Louise Lassalle, Philipp Bräuer, Pierre Aller, Peter T. Docker, Babak Andi, Allen M. Orville, James M. Glowonia, Silke Nelson, Marcin Sikorski, Diling Zhu, Mark S. Hunter, Thomas J. Lane, Andy Aquila, Jason E. Koglin, Joseph Robinson, Mengning Liang, Sébastien Boutet, Artem Y. Lyubimov, Monarin Uervirojnangkoorn, Nigel W. Moriarty, Dorothee Liebschner, Pavel V. Afonine, David G. Waterman, Gwyndaf Evans, Philippe Wernet, Holger Dobbek, William I. Weis, Axel T. Brunger, Petrus H. Zwart, Paul D. Adams, Athina Zouni, Johannes Messinger, Uwe Bergmann, Nicholas K. Sauter, Jan Kern, Vittal K. Yachandra, and Junko Yano. Structure of photosystem II and substrate binding at room temperature. *Nature*, 540(7633):453–457, December 2016. ISSN 0028-0836, 1476-4687. doi: 10.1038/nature20161.